



# Machining characteristics of glass substrates containing chemical components in femtosecond laser helical drilling

Hyeon-Min Lee<sup>1</sup> · Jung-Hyun Choi<sup>2</sup> · Seung-Jae Moon<sup>1</sup>

Received: 16 August 2019 / Revised: 10 May 2020 / Accepted: 11 June 2020 / Published online: 17 July 2020  
© Korean Society for Precision Engineering 2020

## Abstract

The machining characteristics of glass substrates containing chemical components were investigated for the purpose of femtosecond laser helical drilling. A femtosecond laser of wavelength 1552 nm and pulse duration 800 fs was adopted in the laser machining system. The substrates investigated were aluminosilicate, soda-lime, and borosilicate glass. The chemical components contained in each glass substrate were quantitatively analyzed by laser ablation-induced chemical plasma mass spectrometry. The characteristics of the drilling conditions for each glass substrate were affected by its chemical components. As the wt% of Al<sub>2</sub>O<sub>3</sub> and MgO components in the glass substrates increased, the ablation threshold energy of each substrate decreased, resulting in greater vertical speed of the laser head.

**Keywords** Femtosecond laser · Helical drilling · Glass · Glass chemicals

## 1 Introduction

Nowadays, different types of glasses are being used in advanced displays in electronic devices such as mobile phones, tablet personal computers, and laptops. Accordingly, research studies on glass machining methods have been extensively conducted in the electrical devices industry. The conventional mechanical machining of glass substrates causes critical problems, such as cracks, chipping, and random breaking owing to the brittle nature of glass. In the hole drilling of various materials, precise control over mechanical drilling with various tool shapes, spindle revolutions per minute, feed rate, and coolant conditions is needed to achieve good surface quality without cracks and chipping [1–3]. The mechanical drilling process is composed of several steps, such as rough, fine, and finish drilling, which result in increased cost and time. In the mechanical machining process, lubrication oils are needed to reduce the frictional forces and remove burrs. Nowadays, based on the requirements to avoid environmental contamination,

various research reports have been published to determine eco-friendly machining agents instead of conventional lubrication [4, 5] and to minimize the masses of such lubrication oils during machining [6, 7]. Alternatively, laser machining using industrial tap water or pure water can be applied for cooling and removing burrs [8]. In the femtosecond laser machining process, the laser energy is absorbed by the free electrons in the target. The absorbed energy is then thermalized within the electron subsystem and transferred to the lattice, from whence the electron heat is transported into the bulk [9]. The logarithmic dependence of the ablation shape on laser fluence is well known under applications of Gaussian beam shapes [10]. In this logarithmic relationship, the optical absorption coefficient of the solid target determines the thermalization process. This thermal transition process of metals has already been investigated via experiments and simulations in previous studies [10, 11]. The ablation rates for copper and gold were in good qualitative agreement with predictions based on the analytical method involving the two-temperature diffusion model. However, the dielectric glass substrates were almost transparent in the ultraviolet to infrared wavelength range ( $0.21 \mu\text{m} < \lambda < 3.7 \mu\text{m}$ ) [12–14]. This characteristic of a glass substrate limits the use of continuous or even picosecond-pulsed lasers in material modifications. However, ultrashort-pulses of femtosecond lasers can overcome this limit. The ultrashort-pulsed lasers can concentrate high energy densities onto very small areas,

✉ Seung-Jae Moon  
smoon@hanyang.ac.kr

<sup>1</sup> Department of Mechanical Convergence Engineering, Hanyang University, Seoul 04763, Korea

<sup>2</sup> Department of Environmental Science and Engineering, Ewha Womans University, Seoul 03760, Korea

which can then trigger ablation by the multiphoton ionization and impact ionization processes in dielectric materials [15].

Laser drilling methods are generally considered as forms of advanced manufacturing processes, and various drilling methods such as single pulse, percussion, trepan, and helical drilling have been developed [16]. Microsized and tapered holes can be successfully produced on Ni alloy plates of a few millimeters thickness and alumina ceramics using percussion drilling with multiple pulses [17–19]. However, for drilling larger holes with diameters greater than those of typical laser beam spots, the trepan and helical drilling methods are utilized instead of single pulse and percussion drilling. In the helical drilling method, the picosecond laser beam path moves along a circular track on the hole edge, and the circular offset can be fully detached when the stainless-steel plate is drilled through [20]. A high roundness accuracy can be obtained by cutting in the vicinity of the hole edge. The helical drilling method produces a much better surface quality of the sidewall than the trepan drilling method. The vertical motion of the trepan drilling process is generally discontinuous owing to the step-by-step movement in the direction of the substrate thickness. In the helical drilling method, the vertical drilling path of the laser beam is continuous because the circular motion of laser scanning and the vertical motion of the substrate in the direction of the positive  $z$ -axis occur simultaneously.

In these conventional laser drilling methods, the drilling process starts from the top surface of the substrate, resulting in the formation of a recast layer by ablated and accumulated materials. This recast layer can cause spattering and cracks in the thru-holes [21]. To minimize the formation of the recast layer, forced gas flow and underwater submersion can be applied [22]. During the drilling of the thick glass substrate, the focused laser beam can be blocked by the recast layer at the inlet of the hole, resulting in the increase of the taper angles of the thru-holes. The minimization of the taper angle can be achieved when the drilling process is initiated from the bottom of glass substrate in the formation of microsized channels and holes by preventing the formation of the recast layer [23, 24].

In this work, the machining characteristics of glass substrates was investigated in the femtosecond laser helical drilling method starting from the bottom surfaces of the substrates. The glass substrates adopted in this work were aluminosilicate glass (ASG), soda-lime glass (SLG), and borosilicate glass (BSG) substrates, which are widely utilized for advanced displays in electronic devices. The ASG has been known for high strength, high scratch resistance, and long durability [25]. The SLG was widely adopted for liquid-crystal display (LCD) panels and windowpanes because of the characteristics of relatively low price and chemical stability [26]. The BSG has been known for minimized heavy-metal

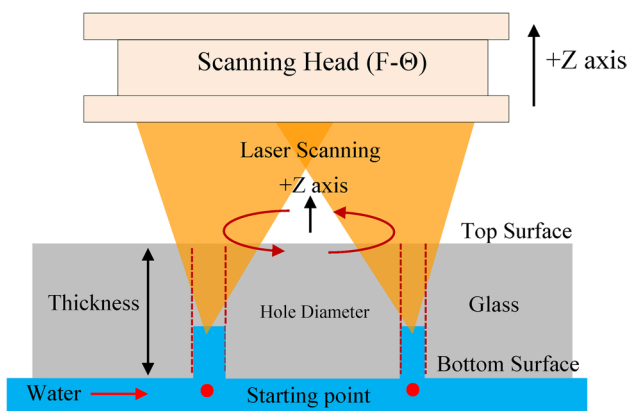
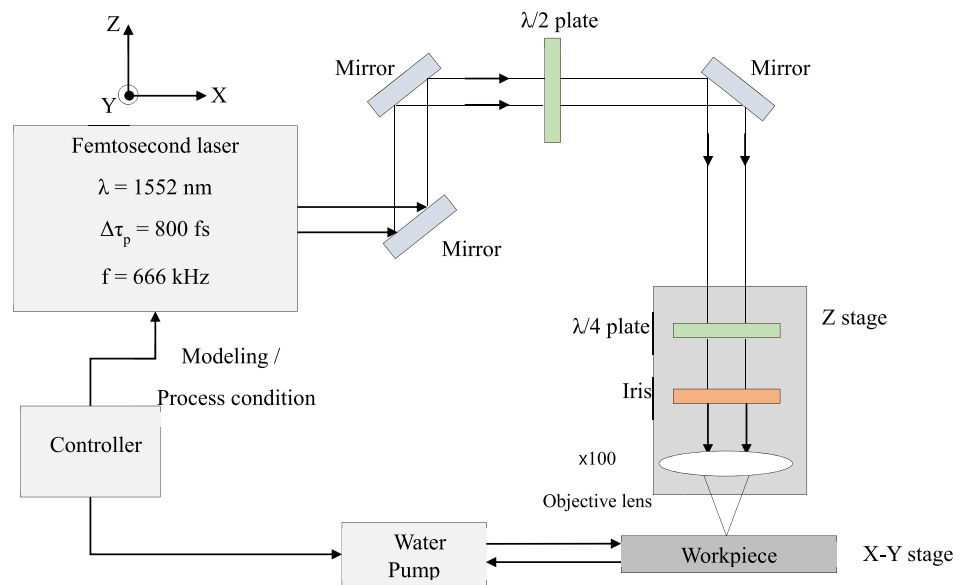
ion inclusion for excellent thermal properties in LCD displays [27]. The differences in the drilling conditions for each glass substrate were extensively investigated and discussed. The chemical ingredients of the adopted industrial glasses were analyzed by laser ablation inductively coupled plasma mass spectrometry (LA-ICP MS). The effects of specific chemical components on the laser helical drilling process were significant.

## 2 Experiments

Experiments were carried out with a laser pulse of 800 fs at a wavelength of 1552 nm with a laser beam diameter of 6  $\mu\text{m}$ . The pulsed laser beam was tightly focused using an objective lens, as can be seen in Fig. 1. The maximum pulse energy was 30  $\mu\text{J}$ , and the maximum pulse-repetition frequency was 660 kHz.

The utilized glass substrates were 400  $\mu\text{m}$ -thick ASG (Corning® Gorilla® glass), 700  $\mu\text{m}$ -thick SLG (Asahi®), and 700  $\mu\text{m}$ -thick BSG (Corning® Eagle XG® glass) substrates. Prior to the analyses of the chemical components in these substrates, they were sufficiently washed using methanol ( $\text{CH}_3\text{OH}$ ) and completely dried with lens tissues and clean air to remove any pollutants from the surface of the substrates. The glass substrate was firmly fixed using a vacuum suction system for the experiment. The top surface of the substrate was positioned in a direction normal to the incoming pulsed laser beam under ambient conditions. The bottom surface was immersed in flowing water, as shown in Fig. 2. The laser energy was measured using an optical power meter before performing the experiment. The surface morphology and quality of the edges in the laser-drilled holes were evaluated using a confocal laser scanning microscope (CLSM; Olympus Co. LEXT OLS 4100 model) with a vertical resolution of 10 nm. The chemical ingredients of each glass substrate were analyzed by LA-ICP MS with irradiation from an ultraviolet yttrium laser at a wavelength of 342 nm, a pulse duration of 500 fs, and a beam size of 75  $\mu\text{m}$ .

The laser helical drilling process is depicted in Fig. 2; the laser beam was focused below the bottom surface of the glass substrate and the laser scanning motion was programmed in the form of a circular path along the hole edge that simultaneously moves in the upper direction, i.e., the positive  $z$ -axis. Consequently, the laser beam follows a helical path from the bottom to the top surface. The laser irradiation should be stopped once the  $z$ -axis motion stops. Otherwise, the top layer of the glass will be irradiated by the laser, which would result in microcracks and chippings around the edge of the hole due to the formation of a thermally affected zone along the edge. The water flow in the trench can help remove glass particles; the water flow was momentarily stopped immediately before hole penetration

**Fig. 1** Schematic of femtosecond laser system**Fig. 2** Process of laser helical drilling method

to prevent overflow of water onto the top surface of the glass substrate, and the circular offcut part was completely detached downward.

### 3 Correlation of laser helical drilling parameters

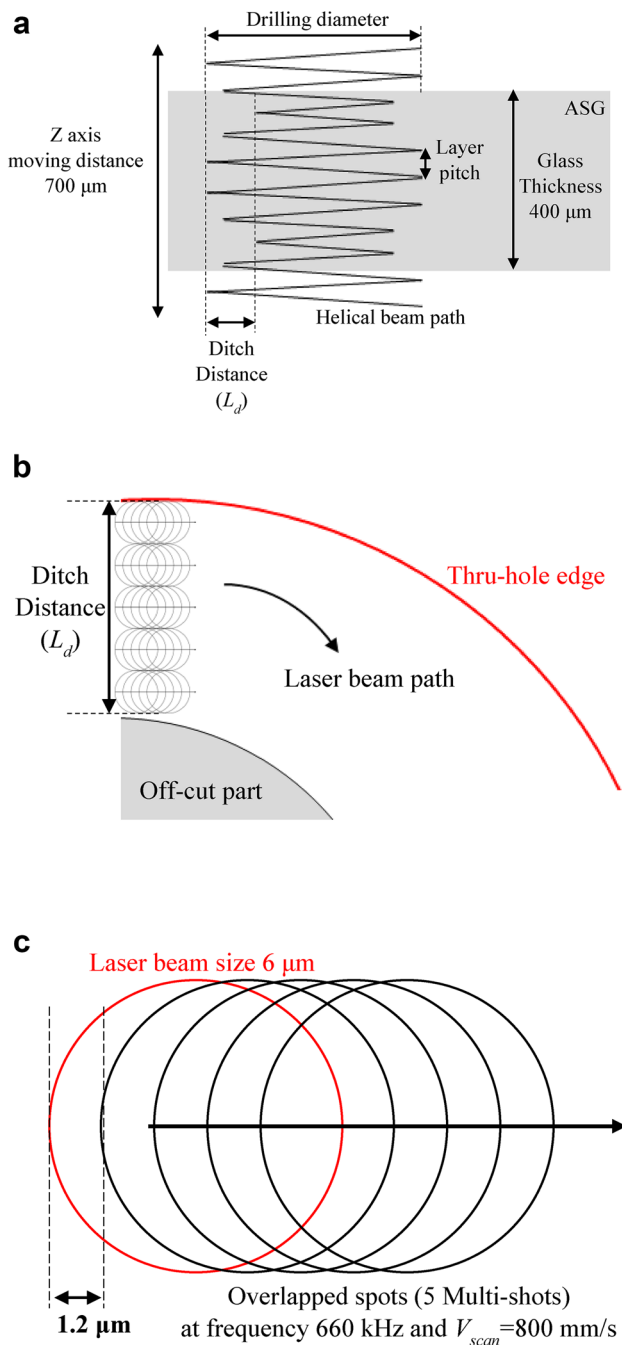
The laser helical beam parameters are shown in Fig. 3. The important helical drilling parameters of the adopted laser system are laser power, frequency, scanning speed, and vertical moving speed. In particular, the helical layer pitch is a critical parameter for determining the penetration and quality of the thru-holes. If the helical layer pitch is larger than the ablation depth of each layer, then each layer will be disconnected and the offcut part cannot be completely removed. The helical layer pitch should thus be smaller than the ablation depth for detaching the offcut

completely. Hence, it is important to determine the appropriate layer pitches and z-axis motion speeds with regard to the ablation depth of each substrate. Additionally, for the purpose of complete drilling, the circular offcut within the laser beam path should be detached without any additional breaking forces. The moving distance in the direction of the positive z-axis should be sufficiently longer than the thickness of the glass, as shown in Fig. 3a. The total z-axis moving distance was multiplied by 1.75 to obtain the original glass thickness for complete penetration of the hole. In the case of the 400 μm-thick ASG substrate, the moving distance was 700 μm. To determine the helical layer pitch, the ablation depth can be calculated from Eq. (1) [28]:

$$L_{\text{depth}} = \alpha^{-1} \ln (F_a / F_{\text{th}}), \quad (1)$$

where  $L_{\text{depth}}$ ,  $\alpha^{-1}$ ,  $F_{\text{th}}$ , and  $F_a$  are the ablation depth, absorption coefficient of the laser wavelength used, ablation threshold laser energy, and incident laser energy in the range of 10–28.3 μJ, respectively.

At scanning speeds greater than 800 mm/s, the number of overlapping laser spots decreased because of increase in the distance between the laser spots. The ablation depth can decrease because of reduction of the number of multiple laser shots on the overlapped area, and the ablation craters in the helical layers cannot be smoothly connected. In contrast, at scanning speeds less than 800 mm/s, because the number of multiple shots increased, the drilling time was increased and more defects were generated around the holes. Therefore, the appropriate scanning speed,  $V_{\text{app\_scan}}$ , was selected as 800 mm/s for connecting the ablation craters. Finally, the relation between the drilling parameters could be summarized using Eq. (2) below:



**Fig. 3** Laser helical drilling parameters

$$L_{\text{scan}} = N\pi DL_d / \phi = a t \pi DL_d / \{ \phi \alpha^{-1} \ln(F_a / F_{\text{th}}) \}, \quad (2)$$

where  $L_{\text{scan}}$ ,  $a$ ,  $t$ , and  $\phi$  are the total scanning distance, coefficient for sufficient moving distance of z-axis direction over the thickness of the glass substrate (i.e., 1.75), glass substrate thickness, and size of the beam spot, respectively. The  $L_{\text{scan}}$  of each glass substrate can be obtained as shown in Fig. 5c. Accordingly, the scanning time,  $T_{\text{scan}}$ , for the thru-hole is determined by Eq. (3):

**Table 1** Laser helical drilling parameters for experiments

Parameters	Values
Laser beam diameter	6 $\mu\text{m}$
Laser frequency	660 kHz
Energy	10–28.3 $\mu\text{J}$
Scanning speed (perimeter speed)	800 mm/s
Z-axis moving speed	0.03–0.2 mm/s
Z-axis moving distance	Glass thickness $\times$ 1.75

$$T_{\text{scan}} = L_{\text{scan}} / V_{\text{app\_scan}} \quad (3)$$

With this scanning time, the z-axis moving speed of  $V_z$  can be obtained using Eq. (4).

$$V_z = a t / T_z = V_{\text{app\_scan}} \phi \alpha^{-1} \ln(F_a / F_{\text{th}}) / \pi D L_d. \quad (4)$$

The ditch distance corresponds to the distance from the thru-hole edge to the offcut part, as shown in Fig. 3b. The ditch distance ( $L_d$ ) in Fig. 3b is necessary for smooth ejection of the removed glass particles by water flow. The  $L_d$  was set as 30  $\mu\text{m}$  in the scanning program. The circular laser beam path along the hole edge was repeatedly changed with five rotations and a spot size of 6  $\mu\text{m}$ . At the maximum laser repetition frequency of 660 kHz and scanning speed of 800 mm/s, five layers of overlapped laser spots can cover an  $L_d$  of 30  $\mu\text{m}$ . In the beam scanning process, the laser beam spot is overlapped as shown in Fig. 3c. The overlapped distance is determined from the spot size and laser frequency. In this work, the overlapped distance between two shots is 4.8  $\mu\text{m}$ , which is approximately 80% of the spot diameter of the laser beam. Table 1 presents the helical drilling parameters used in the experiments.

## 4 Results and discussion

The ablation threshold laser energy,  $F_{\text{th}}$ , of each glass substrate was experimentally determined by the  $D^2$  method, as shown in Fig. 4. The ablation threshold energies were 2.53 J/cm<sup>2</sup> for the ASG, 5.34 J/cm<sup>2</sup> for the SLG, and 7.23 J/cm<sup>2</sup> for the BSG. The threshold energy of the ASG is smaller than those of the SLG and BSG. This is believed to be attributable to the chemical components in each of the glass substrates and will be discussed later. The absorption coefficient,  $\alpha^{-1}$ , was determined by the diffusion length of the conduction band free electrons (CBE) [29]. The CBE diffusion process occurs in 950 fs, which is the summation of the pulse duration of the femtosecond laser (800 fs) and the CBE lifetime (150 fs). The CBE lifetime corresponds to the time required for the recombination of excited electrons and holes. Accordingly, the diffusion length of the CBE is

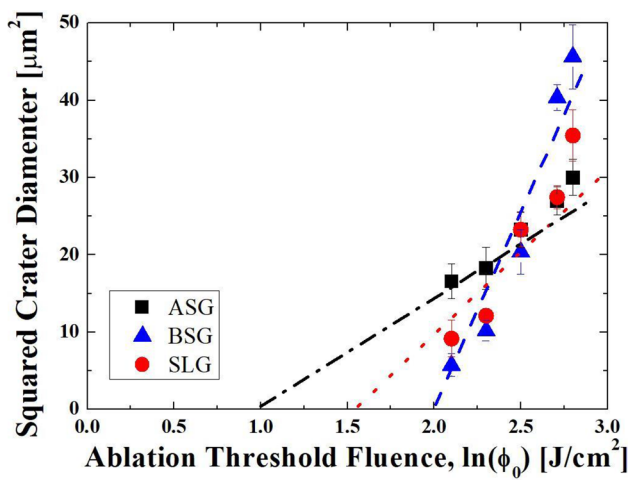


Fig. 4 Ablation threshold fluence of each glass substrate

found to be 950 nm with an approximate CBE velocity of 1 nm/fs [29].

Figure 5a shows the calculated ablation depths for laser energies in the range of 10–28.3 μJ from Eq. (1). As the laser energy increases, the ablation depths of the glass substrates approximately increase from 2.6 to 4 μm in the ASG, 1.8 to 3 μm in the SLG, and 1.5 to 2.5 μm in the BSG. The ablation depth is known to linearly increase with laser shot in femtosecond laser ablation of BSG substrates [30]. The ablation depth of the ASG substrate is longer than those of the SLG and BSG substrates. This is attributable to the lower ablation threshold energy of the ASG substrate. Since the necessary number of helical layers ( $N$ ) are determined from dividing the  $z$ -axis moving distance (ZMD) by the ablation depth of each substrate, the  $N$  for the ASG substrate is lower for complete penetration, as shown in Fig. 5b. The  $N$  of the ASG substrate slowly decreases with increasing laser energy compared with those of the BSG and SLG substrates. The calculated laser scanning distance of each glass substrate,

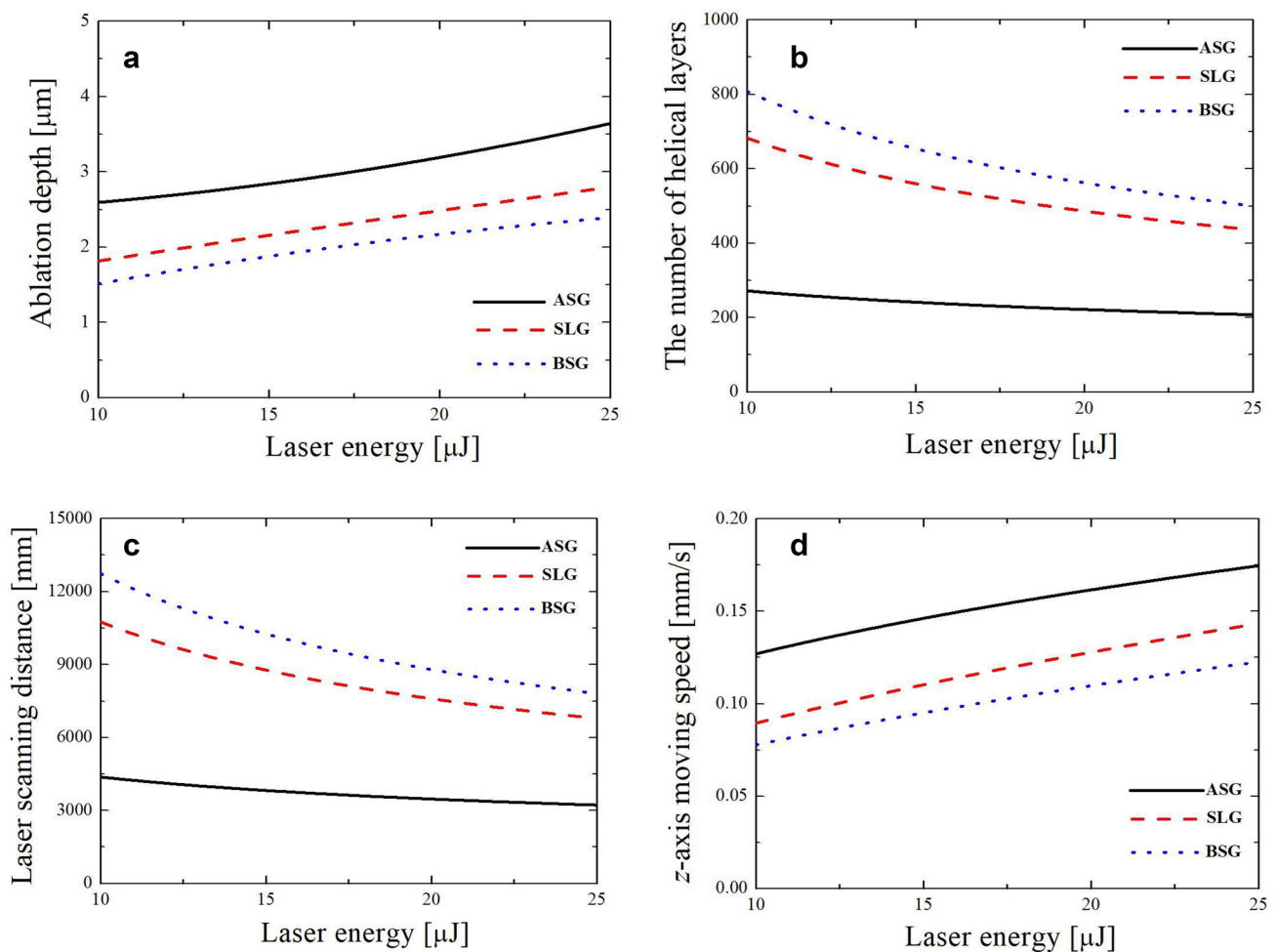


Fig. 5 Helical drilling parameters to vary laser energies: **a** ablation depth, **b** number of helical layers, **c** laser scanning distance, and **d**  $z$ -axis moving speed



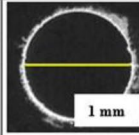
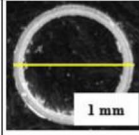
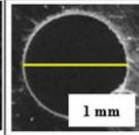
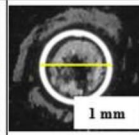
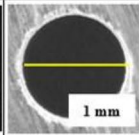
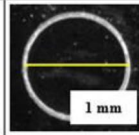
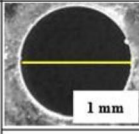
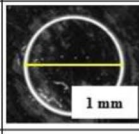
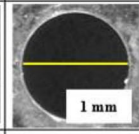
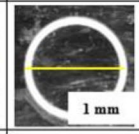
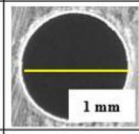
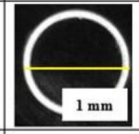
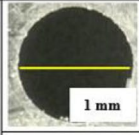
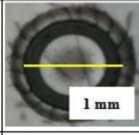
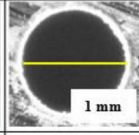
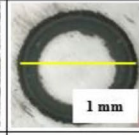
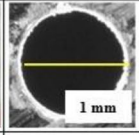
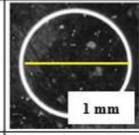
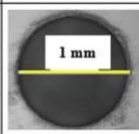
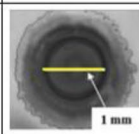
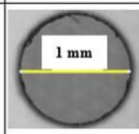

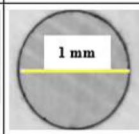
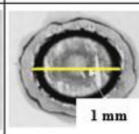
$L_{scan}$ , is presented in Fig. 5c. With the largest ablation depth and lowest number of helical layers, the  $L_{scan}$  of the ASG substrate is the shortest among the three different substrates. The  $L_{scan}$  of the ASG does not vary with the laser energy increase. In Fig. 5d, the calculated vertical moving speeds of the three glass substrates are shown. The ASG has the greatest moving speed compared to the SLG and BSG substrates because the ASG has a larger ablation depth than the SLG and BSG for various laser energies from 10 to 25  $\mu$ J. This larger vertical moving speed of the laser head enables the shortest  $L_{scan}$  in the drilling of the ASG substrate. The  $V_z$  of the ASG was higher by approximately 0.05 mm/s and 0.03 mm/s than those of the BSG and SLG, respectively. The  $V_z$  of each glass was different because the ablated penetration depth of each substrates was different for a given laser energy. The band gap energy of the SLG (2.6 eV) was lower than those of the ASG (3.5 eV) and BSG (3.5 eV) [31, 32]. A low  $V_z$  value indicates that more laser energy is required to connect the crater depth in each helical layer. The used glass substrates are manufactured according to their particular required purpose. Accordingly, the chemical ingredients in each type of glass are specifically engineered.

Figure 6 presents the surface morphology of each glass substrate with a thru-hole diameter of 1 mm and different laser energies in the range of 10–28.3  $\mu$ J. The figure in the left column of each type of glass substrate shows the complete penetration of the thru-holes at the  $V_z$  obtained from

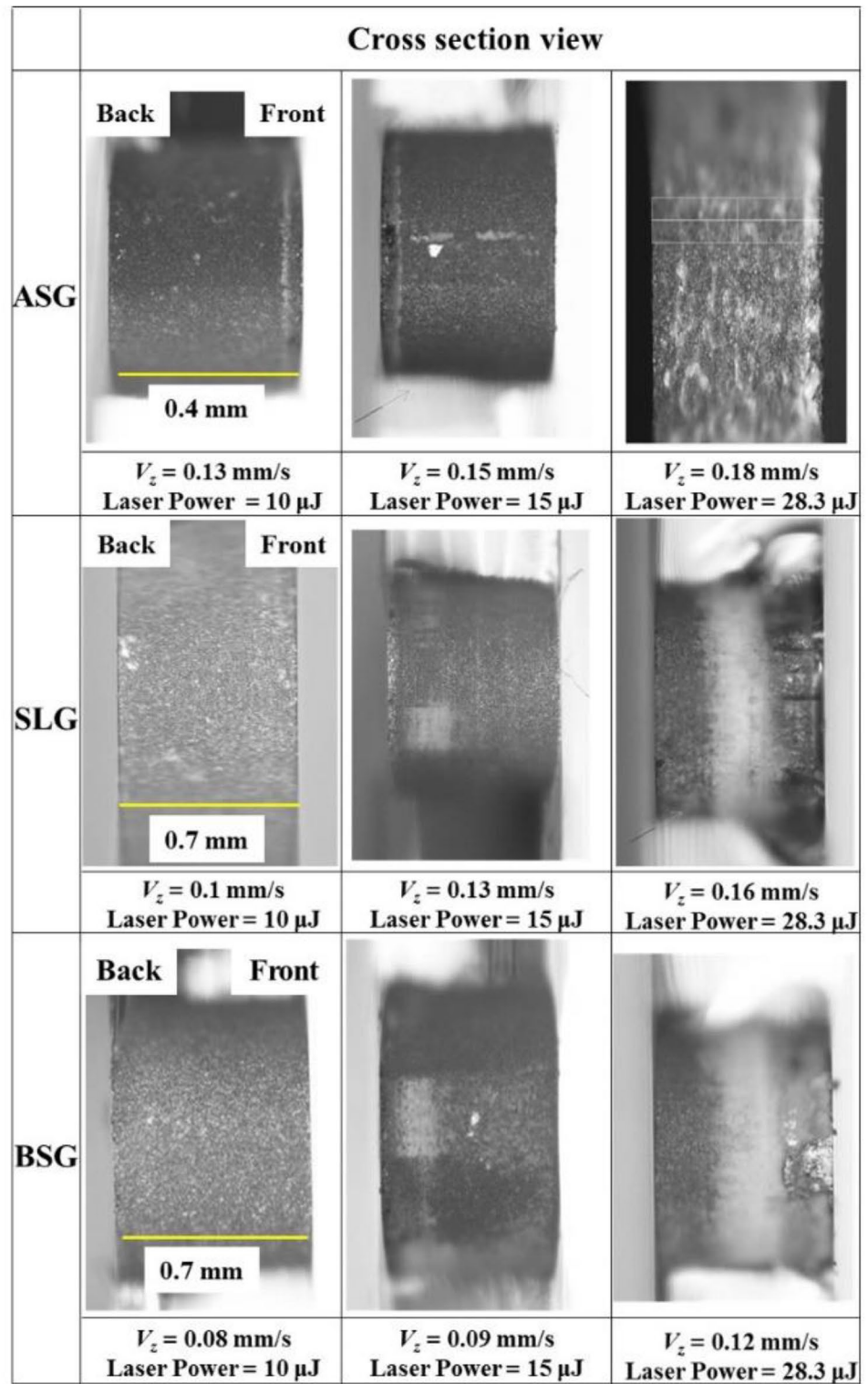
Eq. (4). Only the removed glass particles were observed around the edges of the thru-holes without any cracks or chippings, along with the heat affected zone (HAZ). The figures shown in the right column of each glass substrate present the failed penetrations of the thru-holes at vertical moving speeds greater than  $V_z$ . Specifically, the glass substrate shows the HAZ around the circular beam path for laser energies greater than 20  $\mu$ J. In the case of the ASG and SLG substrate machinings with energies greater than or equal to 20  $\mu$ J, large cracks were observed, as shown in the pictures in the right-side column. Each helical layer was not completely connected owing to the short ablation depth compared to the moving distance at higher speed, and the water flow could not reach the top of the glass through the drilled helical path. As a result, the ablated glass particles could not be extracted, and the glass was affected by excessive thermal accumulation.

Figure 7 shows the surface morphology of the cross-sectional view and the surface roughness. In Fig. 7, small chippings and cracks are observed in the cross-sectional view of the thru-hole fabricated in each type of glass substrate for various  $V_z$  and laser energies. Additionally, the traces of the helical layers were not observed at lower  $V_z$ . This indicates that the layer pitch was large enough to connect and overlap the ablation depths between layers. With high laser energy, the moving speed can be increased.

**Fig. 6** Surface morphology of 1 mm thru-hole diameter by varying laser energy from 5 to 28.3  $\mu$ J

	ASG		SLG		BSG	
10 $\mu$ J						
	$V_z$ 0.13 mm/s	$V_z$ 0.15 mm/s	$V_z$ 0.1 mm/s	$V_z$ 0.12 mm/s	$V_z$ 0.08 mm/s	$V_z$ 0.1 mm/s
15 $\mu$ J						
	$V_z$ 0.15 mm/s	$V_z$ 0.17 mm/s	$V_z$ 0.13 mm/s	$V_z$ 0.15 mm/s	$V_z$ 0.09 mm/s	$V_z$ 0.11 mm/s
20 $\mu$ J						
	$V_z$ 0.17 mm/s	$V_z$ 0.19 mm/s	$V_z$ 0.14 mm/s	$V_z$ 0.16 mm/s	$V_z$ 0.1mm/s	$V_z$ 0.12 mm/s
28.3 $\mu$ J						
	$V_z$ 0.18 mm/s	$V_z$ 0.19 mm/s	$V_z$ 0.16 mm/s	$V_z$ 0.18 mm/s	$V_z$ 0.12 mm/s	$V_z$ 0.14 mm/s

**Fig. 7** Surface morphology of cross section of the thru-hole of each glass substrate for varying laser energy and  $V_z$



However, excessive energy from the high laser energy can cause increased surface roughness.

Figure 8 shows the averaged surface roughness,  $R_a$ , with various values of  $V_z$ . As  $V_z$  was decreased or the deposited laser energy was decreased from 28.3 to 10  $\mu$ J, the average

surface roughness decreased from 0.55 to 0.12  $\mu$ m in the BSG, from 0.55 to 0.18  $\mu$ m in the SLG, and from 0.65 to 0.13  $\mu$ m in the ASG. The surface roughness is maximal at 0.65  $\mu$ m with 0.18 mm/s (28.3  $\mu$ J) for the ASG drilling

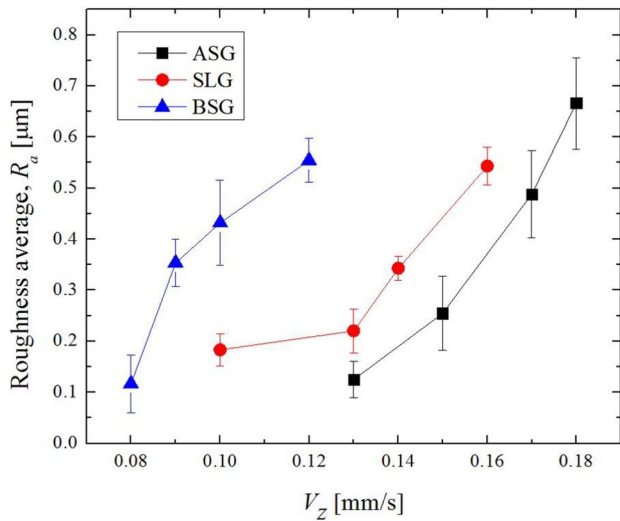


Fig. 8 Average surface roughness for varying  $V_z$

case. This is believed to be affected by the chemical composition of the ASG and will be discussed later.

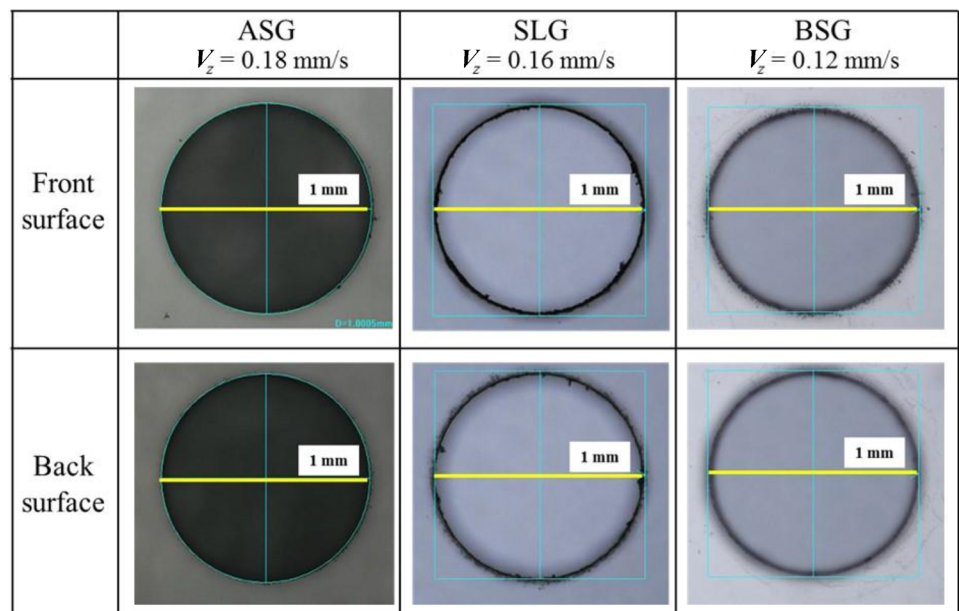
Figure 9 shows the surface morphologies for the top and bottom surfaces and the measured results of the hole diameters in the front and back surfaces in the case of the maximum laser energy of 28.3  $\mu\text{J}$  as the surface roughness was maximized at this energy, as shown in Fig. 8. The corresponding  $V_z$  obtained by Eq. (4) were 0.18 mm/s in the ASG, 0.16 mm/s in the SLG, 0.12 mm/s in the BSG. The diameters of the top and bottom surfaces were almost identical at 1 mm at this high energy without cracks and chippings.

The thru-holes with larger diameters of 2 and 3 mm were successfully fabricated, as shown in Fig. 10. At the

calculated vertical moving speed at the laser energy of 28.3  $\mu\text{J}$ , the  $V_z$  of each glass substrate for the thru-hole diameter of 2 mm was calculated as 0.09 mm/s in the ASG, 0.07 mm/s in the SLG, and 0.05 mm/s in the BSG. In the case of the 3 mm hole diameter, the  $V_z$  of each glass substrate was 0.06 mm/s in the ASG, 0.05 mm/s in the SLG, and 0.03 mm/s in the BSG at an identical laser energy of 28.3  $\mu\text{J}$ . These velocities of the glass substrates were lower than those used for the thru-hole diameter of 1 mm because the ablation depth should be sufficiently interconnected with the increased hole diameter. Some glass particles were adhered around the hole edges; however, there were no significant chippings, cracks, or HAZ in the surface morphology of each condition.

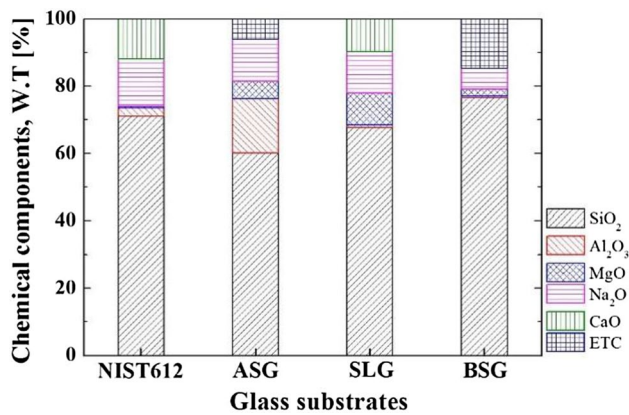
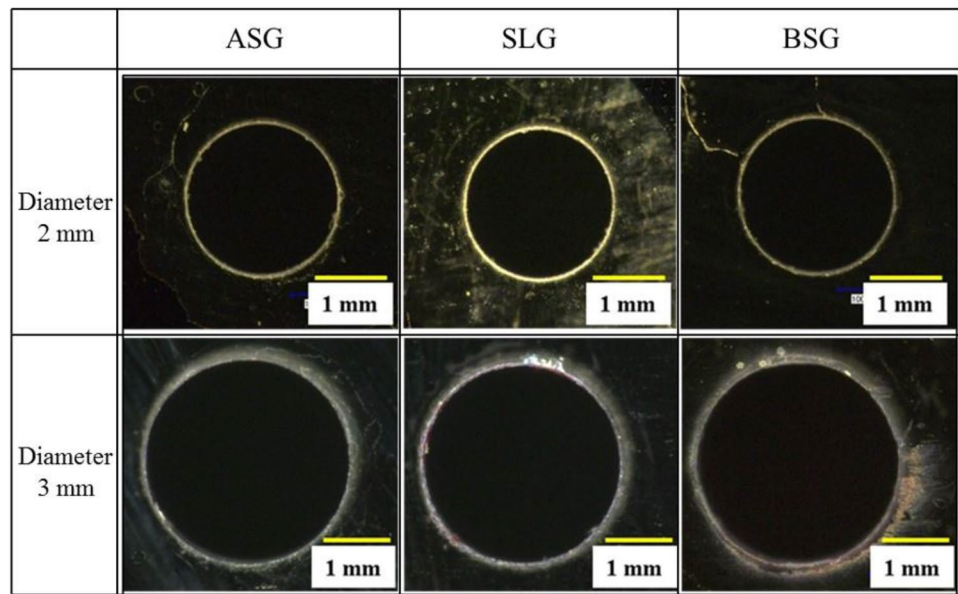
Figure 11 presents the chemical components in each glass substrate measured by LA-ICP MS. The chemical contents of  $\text{SiO}_2$ ,  $\text{Al}_2\text{O}_3$ , and  $\text{MgO}$  were 60%, 14%, and 7% in the ASG, 70%, 2%, and 8% in the SLG, and 78%, 2%, and 0.4% in the BSG, respectively. The LA-ICP MS allows a quantitative analysis of the contents of various chemical components by distinguishing the intensity of each element peak. For the quantitative analysis of each chemical component, the intensity peak values of NIST 612 standard glass measured by LA-ICP MS were used as the reference material. The ablation process in the femtosecond laser machining occurs when the density of free electrons in the conduction band exceeds a specified critical energy density [33]. The  $\text{Al}_2\text{O}_3$  and  $\text{MgO}$  have longer relaxation time scales, which were several tens of picoseconds of excited carriers in the conduction band than the other detected components; for example, the relaxation time of  $\text{SiO}_2$  was known to be 150 fs [34]. Previous research shows that the formation of the self-trapped excitons (STEs) was an important relaxation mechanism in

Fig. 9 Measurement of the hole diameters on the front and back surfaces of each glass substrate





**Fig. 10** Drilling results for 2 and 3 mm hole diameters on each glass substrate



**Fig. 11** Measured chemical components of each glass substrate by LA-ICP MS

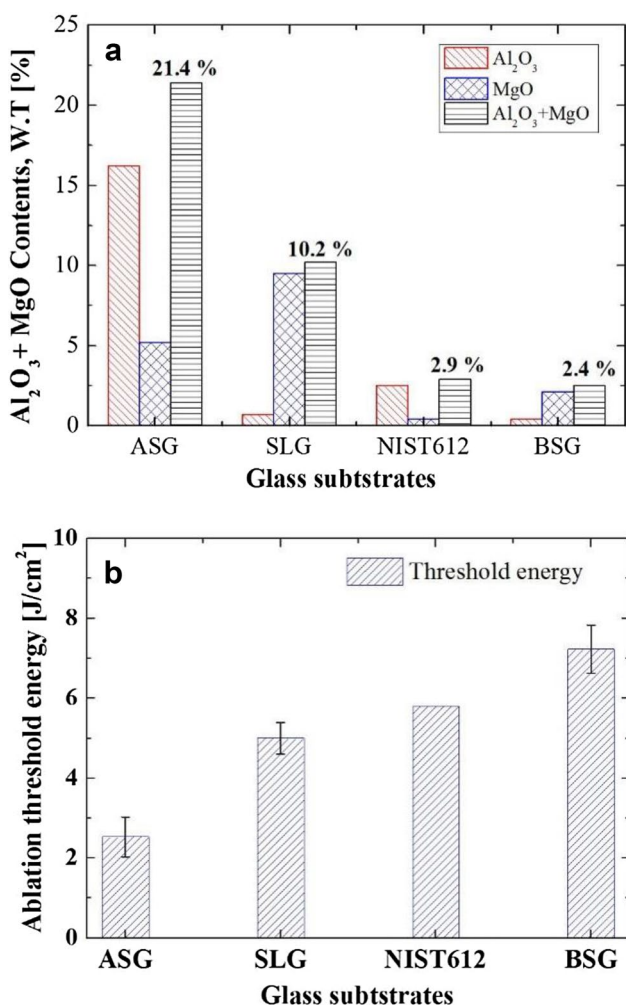
the femtosecond laser processing for wide-bandgap materials. The formation of the STEs means the localization of the thermal energy by the self-trapped carriers. This STE formation suppresses electron excitations [35]. The time scale of the STE formation was known to be approximately 1 ps [35]. The relaxation time of the excited electrons was known to be dependent on the material. In the STE formation mechanism, an electron–hole pair was generally created by the incident radiation of the laser beam. The molecular ion formation results from the self-trapping of a hole in less than 1 ps [34, 35]. An electron excited by femtosecond laser irradiation is then captured by a hole to form the STE. When the STE relaxation time is greater than the lattice relaxation time scale of 10 ps, the released energy from the excited free electrons is converted to the lattice heat energy. This expedites the phonon creation for heat transfer around the

irradiated spot. The containment of Al<sub>2</sub>O<sub>3</sub> and MgO may be conducive to the formation of the HAZ around the ablated crater. If the glass substrates have higher concentrations of Al<sub>2</sub>O<sub>3</sub> and MgO, the ablation process can be initiated at lower threshold energies, and the ablation depths will be longer at the same laser energy from Eq. (1).

Figure 12 shows the contents of Al<sub>2</sub>O<sub>3</sub> and MgO with the ablation threshold energy of each glass substrate. The chemical contents of Al<sub>2</sub>O<sub>3</sub> and MgO were 21.4% in the ASG, 10.2% in the SLG, and 2.4% in the BSG, as seen in Fig. 12a. The ablation threshold energy of the ASG was 2.53 J/cm<sup>2</sup> relatively lower than 5.34 J/cm<sup>2</sup> in the SLG and 7.23 J/cm<sup>2</sup> in the BSG, as given in Fig. 12b. The more the Al<sub>2</sub>O<sub>3</sub> and MgO contents were included, the lesser was the ablation threshold energy required for ablation. Accordingly, the  $V_z$  of the ASG to create the thru-holes was higher by 0.05 mm/s and 0.03 mm/s than the BSG and SLG, respectively.

## 5 Conclusions

The machining characteristics of chemical-containing glass substrates were investigated in the case of femtosecond lasers used for helical drilling. The machining parameters were found to be affected by the chemical components of each of the glass substrates, namely ASG, SLG, and BSG. The thru-holes in the ASG were obtained with higher  $V_z$  than those of the other glass substrates. The  $V_z$  of the ASG was higher than those of the BSG and SLG by 0.05 mm/s and 0.03 mm/s, respectively. The drilling parameters of each type of glass were different according to the chemical components in each glass substrate. In the STE formation mechanism, when the STE relaxation time is greater than the lattice



**Fig. 12** Combined Al<sub>2</sub>O<sub>3</sub> and MgO contents and ablation threshold energy of each glass substrate

relaxation time scale of 10 ps, the released energy from the excited free electrons is converted to lattice heat energy. The Al<sub>2</sub>O<sub>3</sub> and MgO have longer relaxation time scales, which are several tens of picoseconds of excited carriers in the conduction band than the other detected components. The containment of Al<sub>2</sub>O<sub>3</sub> and MgO may thus be conducive to the formation of the HAZ around the ablated crater. The more specific the chemical contents (Al<sub>2</sub>O<sub>3</sub> and MgO) were in the materials, the lower was the ablation threshold energy required, and the thru-holes could be obtained with higher drilling speeds. In our experimental results, the ablation threshold energies of the glass types were 2.53 J/cm<sup>2</sup> in the ASG, 5.34 J/cm<sup>2</sup> in the SLG, and 7.23 J/cm<sup>2</sup> in the BSG. The chemical contents of Al<sub>2</sub>O<sub>3</sub> and MgO were 21.4% in the ASG, 10.2% in the SLG, and 2.4% in the BSG. The ASG had relatively lower threshold energy among the used glass substrates. Accordingly, the ASG substrate can be penetrated with higher  $V_z$  than the BSG and SLG.

**Acknowledgements** This work was partially supported by the National Research Foundation of Korea (NRF) project titled "Development of Coal Analyzing System Using Laser Induced Breakdown Spectroscopy for Clean Coal Power Plant" (no. NRF-2016R1D1A1B03935556). This work was also partially supported by the Basic Science Research Program through the National Research Foundation (NRF) of Korea (no. NRF-2016R1D1A1B04934910).

## Compliance with ethical standards

**Conflict of interest** On behalf of all the authors, the corresponding author states that there are no conflicts of interest.

## References

- Islam MM, Li CP, Ko TJ (2017) Dry electrical discharge machining for deburring drilled holes in CFRP composite. *Int J Precis Eng Manuf Green Technol* 4:149–154
- Qui X, Li P, Li CP, Niu Q, Chen A, Quyang P, Ko TJ (2019) New compound drill bit for damage reduction in drilling CFRP. *Int J Precis Eng Manuf Green Technol* 6:75–87
- Nam JS, Lee SW (2018) Machinability of titanium alloy (Ti–6Al–4V) in environmentally-friendly micro-drilling process with nano-fluid minimum quantity lubrication using nanodiamond particles. *Int J Precis Eng Manuf Green Technol* 5:29–35
- Sen BY, Mia MM, Krolczyk GM, Mandal UK, Mondal SP (2019) Eco-friendly cutting fluids in minimum quantity lubrication assisted machining: a review on the perception of sustainable manufacturing. *Int J Precis Eng Manuf Green Technol*. <https://doi.org/10.1007/s40684-019-00158-6>
- Masoudi S, Esfahani MJ, Jafarian F, Mirsoleimani SA (2019) Comparison the effect of MQL, wet and dry turning on surface topography, cylindricity tolerance and sustainability. *Int J Precis Eng Manuf Green Technol*. <https://doi.org/10.1007/s40684-019-00042-3>
- Iyappan SK, Ghosh A (2020) Small quantity lubrication assisted end milling of aluminium using sunflower oil. *Int J Precis Eng Manuf Green Technol* 7:337–345
- Wang YG, Li CH, Zhang YB, Yang M, Li BK, Dong L, Wang J (2018) Processing characteristics of vegetable oil-based nanofluid MQL for grinding different workpiece materials. *Int J Precis Eng Manuf Green Technol* 5:327–339
- Heo JY, Min HS, Lee MK (2015) Laser micromachining of permalloy for fine metal mask. *Int J Precis Eng Manuf Green Technol* 2:225–230
- Chichkov BN, Momma C, Nolte S, Alvensleben FV, Tünnermann A (1996) Femtosecond, picosecond and nanosecond laser ablation of solids. *Appl Phys A* 63(1):109–115
- Liu JM (1982) Simple technique for measurements of pulsed Gaussian-beam spot sizes. *Opt Lett* 7(5):196–198
- Gamaly EG, Rode AV, Luther-Davies B, Tikhonchuk VT (2002) Ablation of solids by femtosecond lasers: ablation mechanism and ablation thresholds for metals and dielectrics. *Phys Plasmas* 9(3):949–957
- Nolte S, Momma C, Jacobs H, Tünnermann A, Chichkov BN, Wellegehausen WH (1997) Ablation of metal by ultrashort laser pulses. *J Opt Soc Am B* 14(10):2716–2722
- Kitamura R, Pilon L, Jonasz M (2007) Optical constants of silica glass from extreme ultraviolet to far infrared at near room temperature. *Appl Opt* 46(33):8118–8133
- Palik ED (1998) Handbook of optical constants of solids. Academic Express, Red Deer

15. Liu X, Du D, Mourou G (1997) Laser ablation and micromachining with ultrashort laser pulses. *IEEE J Quantum Electron* 33(10):1706–1716
16. Dubey AK, Yadava V (2008) Laser beam machining: a review. *Int J Mach Tools Manuf* 48(6):609–628
17. Li L, Low DKY, Ghosh M, Crookall J (2002) Hole taper characterisation and control in laser percussion drilling. *CIRP Ann Manuf Technol* 51(1):153–156
18. Yan Y, Ji L, Bao Y, Jiang Y (2012) An experimental and numerical study on laser percussion drilling of thick-section alumina. *J Mater Process Technol* 212(6):1257–1270
19. Sezer HK, Li L, Schmidt M, Pinkerton A, Anderson B, Williams P (2006) Effect of beam angle on HAZ, recast and oxide layer characteristics in laser drilling of TBC nickel superalloys. *Int J Mach Tools Manuf* 46(15):1972–1982
20. Zhang H, Di J, Zhou M, Yan Y, Wang R (2015) An investigation on the hole quality during picosecond laser helical drilling of stainless steel 304. *Appl Phys A* 119(2):745–752
21. Mishra S, Yadava V (2015) Laser beam micromachining (LBMM): a review. *Opt Lasers Eng* 73:89–122
22. Tsai C-H, Li C-C (2009) Investigation of underwater laser drilling for brittle substrates. *J Mater Process Technol* 209(6):2838–2846
23. Li Y, Itoh K, Watanabe W, Yamada K, Kuroda D et al (2001) Three-dimensional hole drilling of silica glass from the rear surface with femtosecond laser pulses. *Opt Lett* 26(23):1912–1914
24. Hwang DJ, Choi TY, Grigoropoulos CP (2004) Liquid-assisted femtosecond laser drilling of straight and three-dimensional microchannels in glass. *Appl Phys A Mater Sci Process* 79(3):605–612
25. <https://www.corninggorillaglass.com/>. Accessed Mar 2016
26. [https://www.sid.org/Portals/5/pdf/AGC\\_Asahi\\_Glass\\_DW2013.pdf](https://www.sid.org/Portals/5/pdf/AGC_Asahi_Glass_DW2013.pdf). Accessed Mar 2016
27. <https://www.corning.com/worldwide/en/products/display-glass/products/eagle-xg-slim.html>. Accessed Mar 2016
28. Momma C, Nolte S, Chichkov BN, Alvensleben FV, Tünnermann A (1997) Precise laser ablation with ultrashort pulses. *Appl Surf Sci* 109:15–19
29. Ben-Yakar A, Byer RL (2004) Femtosecond laser ablation properties of borosilicate glass. *J Appl Phys* 96(9):5316–5323
30. Fumitaka M (2015) Micro drilling simulation of ultra-short pulsed laser ablation of glass. *Int J Autom Technol* 9(4):418–424
31. Russ S, Siebert C, Eppelt U, Hartmann C, Faißt B, Schulz W (2013) Picosecond laser ablation of transparent materials. In: *Proceedings of SPIE*, paper no. 86080E, 2013
32. Ruengsri S, Kaewkhao J, Limswan P (2012) Optical characterization of soda lime borosilicate glass doped with TiO<sub>2</sub>. *Proced Eng* 32:772–779
33. Bauerle DW (2011) *Laser processing and chemistry*. Springer, New York
34. Mao S, Quér F, Guizard S, Mao X, Russo R et al (2004) Dynamics of femtosecond laser interactions with dielectrics. *Appl Phys A Mater Sci Process* 79(7):1695–1709
35. Grigoropoulos CP (2009) *Transport in laser microfabrication: fundamentals and applications*. Cambridge University Press, Cambridge

**Publisher's Note** Springer Nature remains neutral with regard to jurisdictional claims in published maps and institutional affiliations.



**Hyeon-Min Lee** is a researcher of Mechanical Engineering at Hanyang University, South Korea. He received his B.Sc. from Jeonbuk National University, South Korea, M.Sc. from Gwangju Institute of Science and Technology, South Korea, and Ph.D. from Hanyang University, South Korea. His research interests include laser machining of ceramic materials, as well as glass manufacturing process design for mass production.



**Jung-Hyun Choi** is a professor of Department of Environmental Science and Engineering at Ewha Womans University, South Korea. She received her B.Sc. from Ewha Womans University, South Korea, M.Sc. and Ph.D. from Princeton University, U.S.A. Her research area covers the fluvial sediment contamination, and development of chemical component analysis method via laser induced breakdown spectroscopy.



**Seung-Jae Moon** is a professor of School of Mechanical Engineering at Hanyang University, South Korea. He received his B.Sc. and M.Sc. from Seoul National University, South Korea, and Ph.D. from University of California, Berkeley, U.S.A. His research interests include laser-material processing, thermal analysis of laser material processing, and laser application for fabrication and instrument in semiconductor fabrication process.